Combined effect of cortical cytoskeleton and transmembrane proteins on domain formation in biomembranes

Md. Kabir Uddin Sikder,[1,a)] Kyle A. Stone,[1,b)] P. B. Sunil Kumar,[2] and Mohamed Laradji[3,c)]

[1]*Department of Physics, The University of Memphis, Memphis, Tennessee 38152, USA*
[2]*Department of Physics, Indian Institute of Technology Madras, Chennai 600 036, India and MEMPHYS – Center for Biomembrane Physics, University of Southern Denmark, DK-5230 Odense, Denmark*
[3]*Department of Physics, The University of Memphis, Memphis, Tennessee 38152, USA and MEMPHYS – Center for Biomembrane Physics, University of Southern Denmark, DK-5230 Odense, Denmark*

(Received 28 February 2014; accepted 25 June 2014; published online 1 August 2014)

We investigate the combined effects of transmembrane proteins and the subjacent cytoskeleton on the dynamics of phase separation in multicomponent lipid bilayers using computer simulations of a particle-based implicit solvent model for lipid membranes with soft-core interactions. We find that microphase separation can be achieved by the protein confinement by the cytoskeleton. Our results have relevance to the finite size of lipid rafts in the plasma membrane of mammalian cells.
 [http://dx.doi.org/10.1063/1.4890655]

I. INTRODUCTION

There currently exists a consensus that the plasma membrane of mammalian cells exhibits lateral heterogeneities in the form of nanoscale domains known as lipid rafts, which are rich in cholesterol and sphingolipids.[1–3] Lipid rafts are believed to serve as platforms for proteins and are implicated in a range of biological functions including signal transduction,[4] endocytosis,[5] trafficking,[6] virus uptake,[7] and regulation of membrane tension.[8,9]

Due to the complexity of the plasma membrane, which results from the presence of a large number of lipid species and membrane proteins as well as various protein-mediated active processes, investigations of the lateral organization of the plasma membrane *in vivo* conditions are experimentally very challenging. To overcome this difficulty, the majority of experimental studies of the lateral organization of biomembranes have been carried out on multicomponent giant unilamellar vesicles (GUVs) and planar membranes composed of a saturated lipid, such as dipalmitoyl phosphatidylcholine (DPPC) or sphingomyelin, an unsaturated lipid, such as dioleyol phosphatidylcholine (DOPC) and cholesterol.[10] These experiments show that μm-scale segregated liquid-ordered (L_o) regions,[11] rich in Chol and saturated lipids, coexist with liquid-disordered (L_d) regions that are rich in unsaturated lipids.[12–19] Since the length scales of these domains extend up to the size of the reconstituted vesicles, one should view these segregated regions as coexisting phases in a thermodynamic sense.[20] Segregated lipid domains in multicomponent GUVs are thus several orders of magnitude larger than lipid rafts in the plasma membrane. Lipid rafts are therefore reminiscent of a microphase separation stabilized by effects that are absent in experimental model membranes.

While the mechanisms which prevent lipid rafts from reaching μm-size domains have been under immense debate, there are some noticeable differences between the plasma membrane and multicomponent GUVs: (1) The transbilayer lipid distribution in the plasma membrane is highly asymmetric with most of the saturated sphingolipids located on the outer leaflet;[21] (2) active lipid recycling to and from the bilayer is present in the case of the plasma membrane while it is absent in reconstituted membranes;[22,23] (3) the plasma membrane contains transmembrane proteins which partition differently in the L_o and L_d domains;[24,25] and (4) the lipid bilayer of the plasma membrane is attached to a subjacent actomyosin cytoskeleton which may lead to the confinement of some transmembrane proteins.[26–28]

Several mechanisms have been postulated to explain the nanoscale of lipid rafts in the plasma membrane. For example, lipid rafts have been hypothesized as compositional fluctuations,[29,30] and the recent study by Veatch *et al.*[30] of GUVs reconstructed from the plasma membrane of rat basophil leukemia cells suggests that the physiological temperature of the plasma membrane is slightly higher than the critical point of the lipid mixture, and thus lipid rafts may be just critical fluctuations. The transbilayer asymmetry of the lipid distribution in the plasma membrane has also been shown, by dissipative particle dynamics (DPD) simulations, to lead to nanoscale domains with a length scale determined by the amount of asymmetry in the transbilayer distribution of the saturated sphingolipids.[31] More recently, it was suggested that mismatch between the spontaneous curvatures of the L_o and L_d monolayers leads to microphase separation in multicomponent membranes.[32] Active lipid recycling has also been shown through coarse-grained simulations of phase-field models to lead to nanoscale domain structures.[33–35] There has also been a proposal that hybrid lipids with one fully saturated

[a)]Permanent address: Department of Physics, Jahangirnagar University, Savar, Dhaka 1342, Bangladesh.
[b)]Current address: Department of Chemical Engineering, Auburn University, Auburn, Alabama 36849, USA.
[c)]Author to whom correspondence should be addressed. Electronic mail: mlaradji@memphis.edu

chain and one partially unsaturated chain may act as a linactant (two-dimensional analog of surfactant) that prefer to locate at the boundaries between regions rich in saturated lipids (and cholesterol) and regions rich in unsaturated lipids.[36] The linactants therefore produce two-dimensional microemulsions with a nanoscale domain structure. Some transmembrane proteins may also act as linactants.[37–40]

The stability of nanoscale lipid rafts has also been hypothesized through the picket-fence model due to Kusumi and co-workers.[26] This model is based on the fact that the plasma membrane is compartmentalized by the actomyosin meshwork into corrals with a length scale 30–40 nm. The effect of these corrals on the diffusion of membrane proteins was demonstrated by an anomalous hop-diffusion of G-protein coupled receptors.[41] The cortical cytoskeleton may therefore act as a pinning agent of the segregating L_o and L_d domains, preventing them from full phase separation. Yethiraj and Weisshaar[42] performed Monte Carlo simulations of a spin-1 Ising model, where the ± 1-spins represent coarse-grained L_o and L_d particles, and the 0-spins, represent transmembrane proteins. The 0-spins are immobile in this model and interact symmetrically with the ± 1-spins. They found that the quenched 0-spins lower the demixing critical temperature and that this decrease is accentuated with increasing the amount of immobile proteins. Similar results were obtained by Gómez *et al.*[43] Ehrig *et al.*[44] used a spin-$\frac{1}{2}$ Ising model to describe the gel-fluid phase separation of distearoyl phosphatodylcholine (DSPC)-dimyristoyl phosphatodylcholine (DMPC) binary mixtures in the presence of a quenched actin cytoskeleton, with average linear corral size of 50 nm. In this model, a fraction of the actin filaments is treated as a quenched field that interacts more favorably with the lipids in the gel phase (i.e., DSPC), and therefore acts as a pinning agent of DSPC. Using Monte Carlo simulations of their model with conserved order parameter, they found that in the absence of cytoskeleton, near-critical compositional fluctuations may lead to transient anomalous subdiffusion. They also found that this subdiffusive behavior is further enhanced when the concentration of the cytoskeleton pinning sites is increased. Furthermore, they found that, in the two-phase region, the cytoskeleton leads to logarithmically slow domain growth, a confirmation that actin, according to this model, acts as a quenched disorder. Even slightly above the critical point, they found that the cytoskeleton leads to some domain structure, due to the affinity between the cytoskeleton and lipids in the fluid state. Machta *et al.*[45] used a similar model to investigate phase separation around the critical temperature of the system and in the presence of a quenched cytoskeleton. The cytoskeleton filaments act as pinning sites for one of the lipid components therefore favoring one of the two liquid phases. They found that the cytoskeleton leads to hop diffusion of the lipids, and even sparsely distributed quenched pinning sites are able to produce microphase separation in the critical region of the phase diagram. In contrast, a higher concentration of pinning sites is needed far from the critical region. Fan *et al.*[34] investigated the kinetics of phase separation using a generalized time-dependent Ginzburg-Landau model and found as well that the cytoskeleton leads to microphase separation. These results are in agreement with recent experiments by Honigmann *et al.*[46] on supported ternary lipid mixtures with binding lipids to actin filament. Both experimental and computational studies with quenched disorder induced by the filamentous actin show that the domain structure mirrors that of the underlying skeleton.

In the studies above, the effect of the cytoskeleton is assumed through either direct interaction between the cytoskeleton and the lipids or mediated by the almost quenched lipids which are anchored to the cytoskeleton, thus acting as a pinning agent of the lipid composition field. A question that arises is whether lipid rafts are also or rather caused by transmembrane proteins that are sterically confined by the cytoskeleton due to their protrusion in the cytoplasmic side of the bilayer.[26] A portion of the actin cytoskeleton is only few nanometers from the lipid bilayer.[47] This part of the cytoskeleton is likely significant in producing membrane corrals, and should sterically hinder the diffusion of membrane proteins that protrude in the cytoplasmic side. The effect that sterically hindered proteins have on the lateral organization of lipids has not been tested previously using explicit models. The purpose of the present study is to specifically investigate the combined effects of these proteins and their confinement by an explicit cytoskeleton on the kinetics of phase separation in multicomponent lipid bilayers, through an explicit model of self-assembled fluid membranes using coarse-grained molecular dynamics simulations.[48] Our results show that the protein confinement leads to slow kinetics of phase separation and microphase separation with an average domain size that decreases with increasing protein confinement and/or increasing their areal number density on the membrane.

The rest of this article is organized as follows. In Sec. II, The implicit-solvent model is introduced and the details of the computational approach are presented. In Sec. III, the simulations results are presented and discussed. Finally, a summary and conclusion are presented in Sec. IV.

II. MODEL AND SIMULATION DETAILS

In order to allow for simulations of large planar membranes and over long timescales, we use a mesoscale implicit-solvent model, developed by us earlier, for self-assembled lipid molecules with soft interactions.[48–50] Here, a lipid molecule is coarse-grained into a semi-flexible short amphipathic chain composed of one hydrophilic (h) bead and two hydrophobic (t) beads. Since we are concerned here with the effect of transmembrane proteins on the phase separation of multicomponent membranes, two types of lipid chains, labeled A and B, are considered. A mimics the unsaturated lipid, while B mimics a mix of saturated lipid and cholesterol. The tail beads of these lipids are labeled t_A and t_B. The head beads of A and B lipids are however identical in this model. This is reasonable, since the phase separation in lipid bilayers is believed to be mainly due to the conformational differences between the saturated and unsaturated tail groups.[51,52]

The upper (cytoplasmic) side of the planar lipid bilayer is underlined with a semi-flexible polymer meshwork

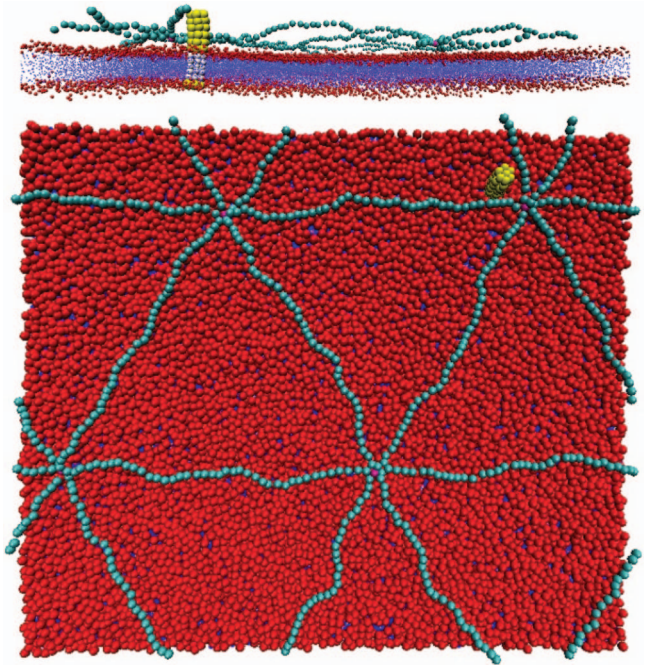

FIG. 1. A snapshot of the model membrane complex showing a one-component lipid bilayer, one protein, and the cytoskeleton. Red and blue beads correspond to lipid head and tail beads, respectively. Yellow beads correspond to the protein's hydrophilic h_p beads, and the gray beads correspond to the proteins hydrophobic, t_p beads. Cyan beads correspond to the cytoskeleton beads, and are also hydrophilic.

tessellated into triangles formed by linking vertices with semi-flexible polymer chains. This polymer meshwork is a simple model for the cortical cytoskeleton and was recently used by us to study cytoskeleton-induced blebbing in biomembranes.[53] The topology of this meshwork is static, and therefore we do not account for the active behavior of the cytoskeleton mediated by myosin motors in this model. For the sake of clarity of the model, both side and top views of the cytoskeleton meshwork together with the self-assembled lipid bilayer are depicted in Fig. 1. The cytoskeleton vertices are anchored to the membrane through a bond with single lipid head groups.

In addition to the lipids and the cytoskeleton, the system also contains transmembrane protein-like clusters of beads, which tend to protrude into the cytoplasm. Our model protein has a cylindrical geometry and is composed of 12 layers of beads, each layer composed of seven beads corresponding to the vertices and center of a hexagon, as shown in Fig. 1. The hydrophobic part of a protein model consists of five layers, each containing seven t_p beads. The exoplasmic (hydrophilic) group of the protein is composed of one layer containing seven h_p beads, and the endoplasmic (also hydrophilic) group of the protein is composed of six layers, to allow its protrusion into the cytoplasm. Somewhat similar protein structures have recently been used earlier.[53]

The interaction potential between beads includes two-body interactions, harmonic interactions for the bonds within a lipid chain, cytoskeleton meshwork, or a protein, and three-body interactions to account for the bending rigidity of a lipid chain, cytoskeleton, or a protein:[48]

$$U(\{\mathbf{r}_i\}) = \sum_{i,j} U_0^{\alpha_i\alpha_j}(r_{ij}) + \sum_i U_{\text{bond}}^{\alpha_i}(r_{i,i+1}) + \sum_i U_{\text{bend}}^{\alpha_i}(\mathbf{r}_{i-1}, \mathbf{r}_i, \mathbf{r}_{i+1}), \quad (1)$$

where $\mathbf{r}_i$ is the position of bead i, $r_{ij} = |\mathbf{r}_j - \mathbf{r}_i|$, and $\alpha_i = h_A$, h_B, t_A, t_B, c, h_P, or t_P, for an A-lipid head bead, a B-lipid head bead, an A-lipid tail bead, a B-lipid tail bead, a cytoskeleton bead, a protein hydrophilic bead, or a protein hydrophobic bead, respectively. In Eq. (1), $U_0^{\alpha_i\alpha_j}$ is a soft two-body interaction between two beads i and j and is given by

$$U_0^{\alpha\beta}(r) = \begin{cases} \left(U_{\max}^{\alpha\beta} - U_{\min}^{\alpha\beta}\right)\frac{(r_m - r)^2}{r_m^2} + U_{\min}^{\alpha\beta} & \text{if } r \le r_m, \\ -2U_{\min}^{\alpha\beta}\frac{(r_c - r)^3}{(r_c - r_m)^3} + 3U_{\min}^{\alpha\beta}\frac{(r_c - r)^2}{(r_c - r_m)^2} & \text{if } r_m < r \le r_c, \\ 0 & \text{if } r > r_c. \end{cases} \quad (2)$$

Here, $U_{\max}^{\alpha\beta} > 0$ for any pair (α, β). Since the solvent is not explicit in this model, the self-assembly of the lipid chains is achieved through making the interaction between lipid tail beads attractive at intermediate distances, i.e., $U_{\min}^{\alpha\beta} < 0$ for $(\alpha, \beta) = (t_k, t_l)$ for any values of k and l. Otherwise, the interaction between two lipid head beads or between a tail and a head bead is fully repulsive, i.e., $U_{\min}^{\alpha\beta} = 0$ if either α or $\beta = h$. The interaction between two non-bonded cytoskeleton beads and the interaction between a cytoskeleton bead and a lipid bead is assumed repulsive. The hydrophobic beads of a protein interact attractively with the lipids tail beads, i.e., $U_{\min}^{\alpha\beta} < 0$ for $(\alpha, \beta) = (t_k, t_P)$ or (t_P, t_k), for $k = A$, B, or P. Otherwise, the interaction between a protein bead and any other bead is assumed repulsive.

The potential U_{bond}^{α} ensures the connectivity between two consecutive monomers in a lipid chain, cytoskeleton, or protein and is given by

$$U_{\text{bond}}^{\alpha_i\alpha_j}(r_{ij}) = \frac{k_{\text{bond}}}{2}(r_{ij} - a_b)^2, \quad (3)$$

where k_{bond} is the bond stiffness coefficient and a_b is the preferred bond length. Both parameters are assumed to be the same for all bonds.

U_{bend}^{α} is a three-body interaction potential ensuring bending stiffness of a lipid chain, cytoskeleton, or protein, and is given by

$$U_{\text{bend}}^{\alpha_i\alpha_j\alpha_k}(\mathbf{r}_i, \mathbf{r}_j, \mathbf{r}_k) = \frac{k_{\text{bend}}}{2}\left(\cos\theta_0 - \frac{\mathbf{r}_{ij}\cdot\mathbf{r}_{jk}}{r_{ij}r_{jk}}\right)^2, \quad (4)$$

where k_{bend} is the bending stiffness coefficient of any triplet of connected beads belonging to a lipid chain, cytoskeleton, or a protein, and is assumed to be independent of the molecular species. θ_0 is the preferred splay angle and is chosen as 180° for all triplets belonging to either lipid or cytoskeleton chains. However, $\theta_0 = 60°, 90°, 120°$, or 180° in the case of protein beads, depending on the triplet in a protein. This will ensure a relatively rigid structure of protein particles.

The values of the various interaction parameters used in the present simulations are given by

$$\begin{aligned}
U_{\max}^{\alpha\beta} &= 100\epsilon \text{ unless } \alpha \text{ and } \beta = t_A,\ t_B \text{ or } t_P,\\
U_{\max}^{t_A t_A} &= U_{\max}^{t_B t_B} = U_{\max}^{t_A t_B} = 200\epsilon,\\
U_{\min}^{\alpha\beta} &= 0 \text{ unless } \alpha \text{ and } \beta = t_A,\ t_B \text{ or } t_P,\\
U_{\min}^{t_A t_A} &= U_{\min}^{t_B t_B} = -6\epsilon,\\
U_{\min}^{t_A t_B} &= -5.5\epsilon,\\
U_{\min}^{t_A t_P} &= -6\epsilon,\\
U_{\min}^{t_B t_P} &= -5.8\epsilon,\\
k_{\text{bond}} &= 100\epsilon/r_m^2,\\
k_{\text{bend}} &= 100\epsilon,\\
a_b &= 0.7r_m.
\end{aligned} \tag{5}$$

In the present study, $a_b = 1.01$ nm for a cytoskeleton bond. The number of bonds in the cytoskeleton between two anchors, N_c, is varied between 10 and 40. All simulations were performed on membranes with constant area. The membrane's linear size along the x-axis is $L_x = 167.20$ nm and its dimension along the y-axis is $L_y = L_x \tan(\pi/3)/2$. Note that $L_x \neq L_y$ in these simulations due to the use of periodic boundary conditions and the need to preserve the triangular symmetry of the cytoskeleton. The lipid number density in the simulations is $\sigma_0 = 3.1\ \text{nm}^{-2}$ (which corresponds to 75 050 lipids in a bare membrane case). We note that a bare membrane with this lipid number density is tensionless. We considered cases where the numbers of cytoskeleton anchors to the bilayer, n_a, is 16, 64, and 256, corresponding to corrals with average linear size $L_c = 41.80$ nm, 20.90 nm, and 10.45 nm, respectively.

The proximity of the cytoskeleton to the bilayer is controlled by varying the number of monomers between two anchors while keeping the average corral size constant. We define a proximity parameter, $\gamma_c = D_c/L_c$, where D_c is the contour length of a cytoskeleton filament between two anchors. A small γ_c corresponds to a cytoskeleton that is fairly close the bilayer, whereas a large γ_c corresponds to a cytoskeleton with large conformational fluctuations from the bilayer. We considered cases where $\gamma_c = 1.06$, 1.43, 1.91, and 2.24, corresponding to average distances of the cytoskeleton from the lipid head groups, of the upper leaflet, varying between 1.6 nm and 4.4 nm. An increase in the fluctuations of the cytoskeleton leads to a decrease in the steric hindrance that it exerts on the proteins.

In all simulations, the area fraction of the majority lipid, $\phi_B = 70\%$. When the amount of proteins is varied, the amount of A-lipids is varied such as $\phi_A + \phi_P = 30\%$.

Three sets of simulations were performed: (1) Set A is used to investigate the effect of protein number density, while the average corral size, L_c, is fixed. Here, we consider the case where $L_c = 10.45$ nm (corresponding to 256 anchors) and the cytoskeleton proximity parameter is fixed at $\gamma_c = 1.06$. The number of transmembrane proteins here are $N_p = 0$, 50, 100, 200, and 400, which correspond to an area fraction of 0%, 0.625%, 1.25%, 2.5%, and 5%, respectively. (2) Set B is used to investigate the effect of cytoskeleton's proximity for a fixed number of proteins $N_p = 400$ and average linear corral size, $L_c = 10.45$ nm. Here, we consider cytoskeleton filaments with proximity parameter $\gamma_c = 1.06$, 1.43, 1.91, and 2.24. (3) Set C is used to investigate the effect of the linear size of the cytoskeleton corral for a fixed number of proteins, $N_p = 400$, and a fixed cytoskeleton proximity parameter, $\gamma = 1.06$. Here, we consider average linear corral size $L_c = 10.45$ nm, 20.90 nm, and 41.80 nm. We emphasize that in the present model, the cytoskeleton affects phase separation indirectly through steric hindering of the diffusion of the transmembrane proteins. This is contrasted with previous studies[34,43–45] where the cytoskeleton directly interacts with the lipids.

The simulations are performed as follows: a single component lipid bilayer, composed of A-lipids with transmembrane protein and cytoskeleton, is initially equilibrated over a long time. Randomly picked lipid molecules with the desired volume fraction are then switched to B-lipids, triggering the onset of phase separation. Domain growth is monitored through three measures: (1) The first length scale of the domain structure is extracted from the compositional structure factor defined as

$$S(q_\parallel, t) = \langle |\tilde{\phi}(\mathbf{q}_\parallel, t)|^2 \rangle, \tag{6}$$

where $\mathbf{q}_\parallel = (q_x, q_y)$ and

$$\begin{aligned}
\tilde{\phi}(\mathbf{q}_\parallel, t) = \int d\mathbf{r}_\parallel e^{i\mathbf{q}_\parallel \cdot \mathbf{r}_\parallel}\\
\times (\phi_A(\mathbf{r}_\parallel, t) + \phi_P(\mathbf{r}_\parallel, t) - \phi_B(\mathbf{r}_\parallel, t)),
\end{aligned} \tag{7}$$

where $\mathbf{r}_\parallel = (x, y)$, and $\phi_A(\mathbf{r}_\parallel, t)$, $\phi_B(\mathbf{r}_\parallel, t)$, and $\phi_P(\mathbf{r}_\parallel, t)$ are the local volume fractions of the components A, B and proteins at time t, respectively. A domain size, $R_2(t)$, is extracted from the second moment of the compositional structure factor,

$$R_2(t) = 2\pi \left(\sum_{q_\parallel = 2\pi/L_x}^{q_c} S(q_\parallel, t) \Big/ \sum_{q = 2\pi/L_x}^{q_c} q_\parallel^2 S(q_\parallel, t) \right)^{1/2}, \tag{8}$$

where q_c is a cutoff wave vector taken to be $2.5r_m^{-1}$.

(2) The average domain area, $A_D(t)$, is extracted from the domain area distribution, $P(\mathcal{A}, t)$, where $\mathcal{A}$ is the domain area:

$$A_D(t) = \int P(\mathcal{A}, t)\mathcal{A} d\mathcal{A}. \tag{9}$$

Domains are determined numerically by subdividing the system's area into small squares of linear size $1.5r_m$. A square is then filled if it contains a bead that belongs to lipid A or protein. Otherwise, the square is empty. Two filled squares belong to the same cluster if they are nearest neighbors.

(3) To quantify the anisotropy of the domains, we also measured the quantity $S(t) = l_D(t)/\sqrt{A_D(t)}$, where l_D is the average perimeter length of a single domain. The perimeter of a domain is defined by the number of filled squares, as defined above, that are along the contour of a domain.

III. RESULTS

A. Protein confinement by the cytoskeleton

To demonstrate that the present model allows for the confinement of proteins by a relatively tight cytoskeleton, we made simulations of one-component lipid bilayers (composed of *A*-lipids only) with proteins and cytoskeleton. The density profiles of the various types of beads in the membrane are shown in Fig. 2 for both cases of a tight cytoskeleton ($\gamma_c = 1.06$) and a loose cytoskeleton ($\gamma_c = 2.24$). Fig. 2(a) shows that in the case of a tight cytoskeleton ($\gamma_c = 1.06$), the distribution of the hydrophilic part of the proteins within the cytoplasm is broader than that of the cytoskeleton beads, which implies that in this case the proteins are well confined by the cytoskeleton. This is consistent with the fact that in this case, the cytoskeleton filaments are 1.6 nm from the head groups of the upper leaflet of the lipid bilayer. In contrast, Fig. 2(b) shows that in the case of a loose cytoskeleton ($\gamma_c = 2.24$), the width of the distribution of the cytoskeleton beads extends beyond that of the hydrophilic beads of the proteins within the cytoplasmic side of the membrane, implying that in this case the proteins are not well confined. In this case the cytoskeleton is in average 4.4 nm from the head groups of the upper leaflet of the lipid bilayer, but extending up to 10 nm from the top leaflet, implying that proteins can easily escape the corrals in this case as compared to the case of $\gamma_c = 1.06$.

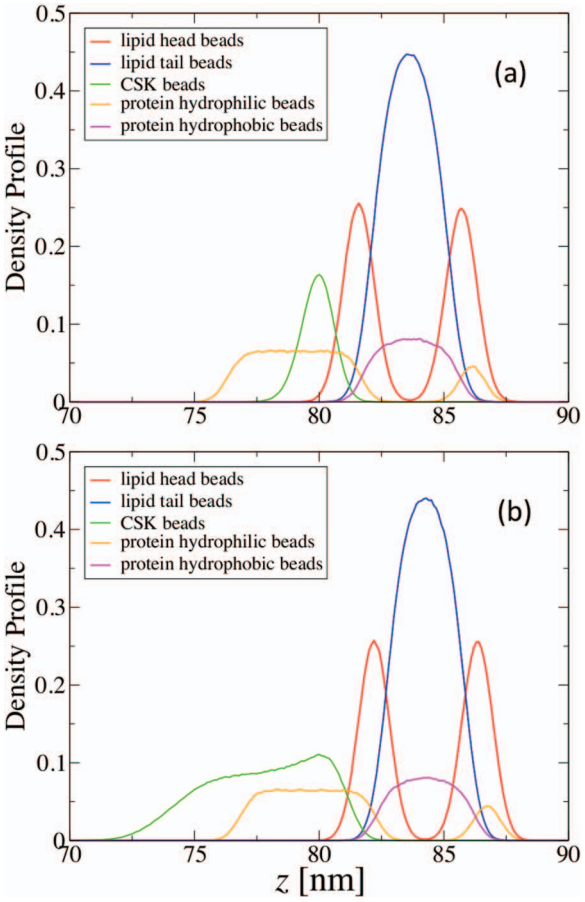

FIG. 2. Density profiles of the various types of beads in the system. Panel (a) corresponds to the case of a tight cytoskeleton, $\gamma_c = 1.06$, and (b) corresponds to the case of a loose cytoskeleton, $\gamma_c = 2.24$.

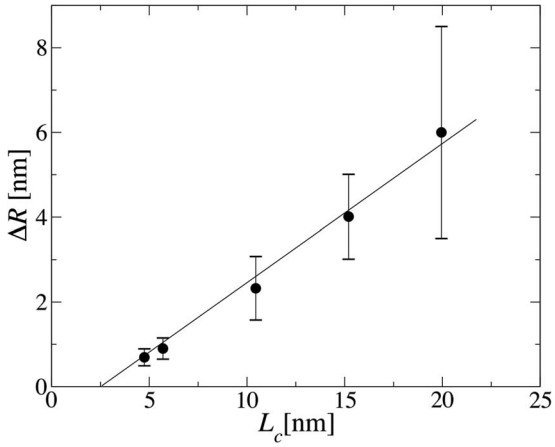

FIG. 3. The asymptotic value of the root mean square displacement, ΔR, for the case of a tight cytoskeleon, $\gamma_c = 1.06$, vs. the average corral size, L_c.

In order to quantify the confinement of proteins, we also looked at their diffusion through the mean square displacement of a protein's center of mass in a one-component lipid bilayer, $(\Delta R_{CM}(t))^2 = \langle(\mathbf{R}_{CM}(t + t_0) - \mathbf{R}_{CM}(t_0))^2\rangle$. The confinement length, defined as $\lim \Delta R_{CM}(t)$ as $t \to \infty$, as a function of γ_c is shown in Fig. 3. We found that in the case of a tight cytoskeleton, $\gamma_c = 1.06$, the mean square displacement reaches a plateau. However, finite diffusion coefficients are found for $\gamma_c = 1.43$, 1.91, and 2.24. Fig. 3 shows that the asymptotic value of ΔR_{CM}, in the case of $\gamma_c = 1.06$, is proportional to the average corral size, L_c, implying that the proteins are indeed confined by the cytoskeleton.

B. Effect of protein density on the kinetics of domain growth

In this section, we present results pertinent to the effect of protein number density on the phase separation process of multicomponent lipid bilayers. We recall that we consider here the case of transmembrane proteins that interact more attractively with *A*-lipids than *B*-lipids. This is motivated by the work of Lillemeier *et al.*, where they found that most of transmembrane proteins have an affinity to cholesterol rich regions.[28]

In Fig. 4, time sequences of snapshots of Set A systems containing 50, 200, and 400 transmembrane proteins are shown. These snapshots show that the proteins and the cytoskeleton have a dramatic effect on both the kinetics of domain growth and the domains morphology. In particular, Fig. 4 shows that in the case of small amount of proteins, $N_P = 50$ (cf. snapshot sequence of column (a)) domains are more circular than in the cases of $N_P = 200$ (column (b)) and $N_P = 400$ (column (c)). The shape of the domains becomes increasingly irregular with increasing the number density of proteins. Furthermore, Fig. 4 qualitatively shows that the growth rate is slowed down with increasing protein density. In particular, we note that at late times, the domains structure hardly evolves in systems with 200 and 400 proteins, implying that the proteins are acting as a pinning agent for domain growth.

The early dynamics of the phase separation process here proceeds as a result of the instability of long wavelength

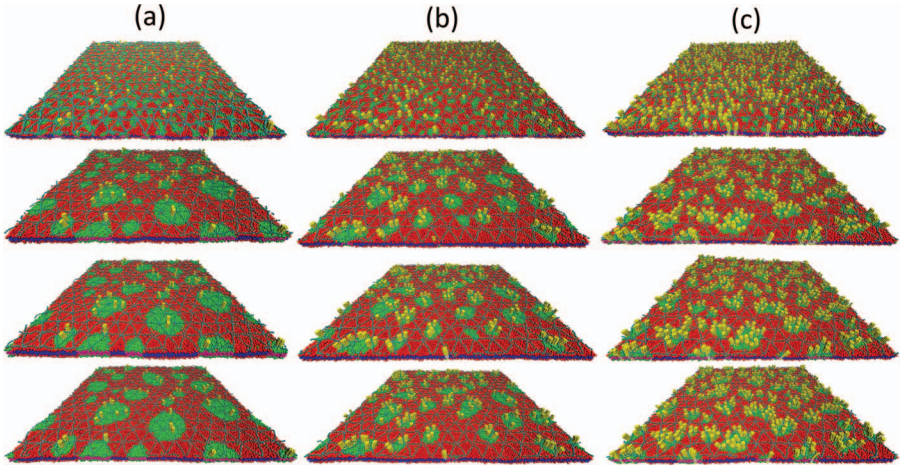

FIG. 4. Snapshot series for Set A systems containing 50 proteins (a), 200 proteins (b), and 400 proteins (c). Snapshots from top to bottom correspond to 200τ, $40\,000\tau$, $60\,000\tau$, and $80\,000\tau$, respectively. Yellow corresponds to protein beads, cyan corresponds to the cytoskeleton. Red corresponds to the head beads of the majority lipid, and green corresponds to the head beads of the minority lipid.

compositional fluctuations, as opposed to nucleation, due to the relatively large volume fraction of the minority *A*-lipid (we note that the volume fraction of *A*+proteins is 30%, which falls within the regime of spinodal decomposition instead of nucleation). The fluctuations eventually become well-defined compact domains at early times. Due to the affinity between *A*-lipids and proteins, a fraction of these domains contain proteins. While the domains that do not contain proteins are free to diffuse, the diffusion of protein-containing domains becomes restricted by the proteins being confined by the cytoskeleton, as shown by Fig. 4. The more mobile protein-free domains eventually merge with protein-containing domains since Fig. 4 shows that all domains at late times contain proteins in the cases of $N_P = 200$ or 400.

The average domain size as calculated from the second moment of the structure factor, i.e., using Eq. (8), is shown in Fig. 5 for Set A systems. Also shown in this figure are the average domain sizes of a pure binary mixture (i.e., where both proteins and cytoskeleton are absent) and the case of 400 proteins but without cytoskeleton. This figure quantitatively shows that the presence of both proteins and cytoskeleton leads to a dramatic slowing down of the kinetics at late times. Furthermore, Fig. 5 shows that growth is further slowed down as the amount of proteins is increased, in agreement with Fig. 4, and that the domain size at saturation decreases with increasing protein content in the membrane.

Fig. 5(b) shows that, in the absence of cytoskeleton and proteins, $R_2(t)$ grows algebraically in time, i.e., $R_2 \sim t^{\alpha}$, with the exponent $\alpha \approx 0.2$. Previous simulations of domain growth of lipid domains using DPD have shown that in the case where domains are compact, the average domain size, $R(t) \sim t^{\alpha}$ with $\alpha = 1/3$.[54–56] This discrepancy is due to the lack of hydrodynamics in the present study, whereas DPD fully takes into account hydrodynamic interactions.[57] Indeed, in the present model, the ambient solvent is not present explicitly and the equations of motion do not conserve local momentum. Hydrodynamics are therefore absent in these simulations. Earlier scaling arguments by Binder and Stauffer,[58] for phase-separating binary mixtures where compact domains grow via their random diffusion and coalescence without hydrodynamics, lead to a growth law, $R \sim t^{1/(3+\mathcal{D})}$, where $\mathcal{D}$ is the spatial dimension. Therefore, $R \sim t^{0.2}$ for $\mathcal{D} = 2$, which is in very good agreement with our simulation results in the absence of cytoskeleton. In the presence of proteins, with $N_P = 400$, but without cytoskeleton, domain growth is also

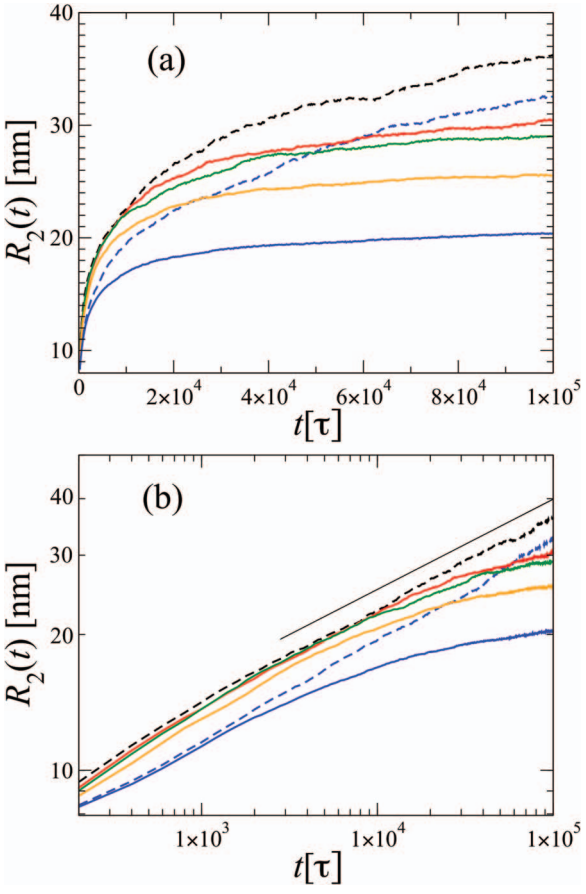

FIG. 5. (a) Domain size, as defined from the second moment of the structure factor vs. time for Set A simulations. The top dotted line corresponds to a pure binary mixture and the bottom dotted line corresponds to a system containing 400 proteins but without cytoskeleton. The solid lines from top to bottom correspond to 50, 100, 200, and 400 proteins, respectively. (b) Same data as in (a) presented in a double logarithmic plot. The slope of the straight solid black line is 0.2.

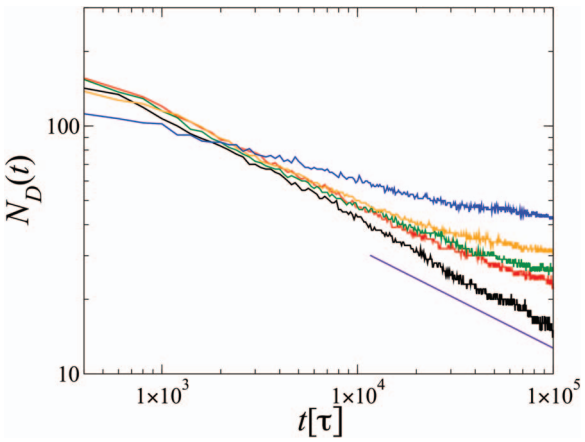

FIG. 6. Number of domains vs. time in the case of Set A. The black curve corresponds to the system with 400 proteins but without cytoskeleton. The other curves from bottom to top correspond to $N_P = 50$, 100, 200, and 400, respectively. The slope of purple line is −0.4.

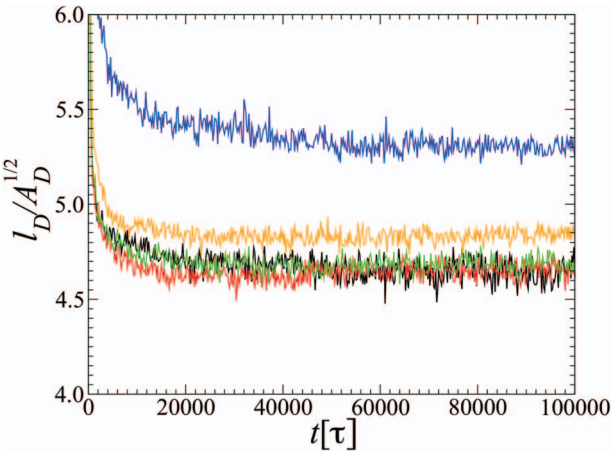

FIG. 7. Average domains perimeter over the square root of the domain area, $l_D(t)/\sqrt{A_D(t)}$, in the case of Set A. Black curve corresponds to a pure binary bilayer. Red, green, orange, and blue curves correspond to $N_P = 50$, 100, 200, and 400, respectively.

algebraic with same exponent, $\alpha \approx 0.2$, except that in this case the prefactor of the power law is smaller. This is expected since proteins are bulkier and their diffusivity is lower than that of lipid molecules, thereby reducing the overall diffusion of domains composed of *A*-lipids and proteins. Similar results were found earlier in molecular dynamics simulations of the effect of nanoparticles on spinodal decomposition of fluid mixtures.[59] The results of Fig. 5 are substantiated by Fig. 6, which shows the number of domains, $N_D(t)$ as a function of time. This figure shows that in the absence of cytoskeleton, the number of domains grows algebraically with time, $N_D \sim t^{-\beta}$ with $\beta \approx 2\alpha$. This is expected since the total area covered by the domain is constant, and therefore, $N_D(t)R_2^2(t) \sim const$. In the presence of cytoskeleton and proteins, however, $N(t)$ decays slower and non-algebraically, in line with the results of Fig. 5. Fig. 6 also shows that the number of domains increases with increasing the number of proteins.

The domains anisotropy, defined here as $S(t) = l_D(t)/\sqrt{A_D(t)}$ (where l_D and A_D are the average perimeter length and area of a single domain, respectively) is shown as a function of time in Fig. 7. This figure shows that in the case of 0, 50, and 100 proteins, $S(t)$ is almost independent of the number of proteins at late times, and that it saturates fairly early during the kinetics. This indicates that the domains assume almost circular shapes early in the dynamics, and that the addition of small amounts of protein, although slows down and eventually arrests domain growth, does not affect the overall domain structure. Fig. 7 shows that the value of $S(t)$ at saturation during late times increases with increasing N_P, implying an increase in the irregularity of the domains shape as N_P is increased. This is qualitatively substantiated by Fig. 4.

C. Effect of cytoskeleton proximity and average corral size on the kinetics of domain growth

Since the cytoskeleton proximity affects the confinement of the proteins, as shown by Figs. 1 and 2, an effect of this on domain growth is also expected. Snapshots at $t = 20\,000\tau$

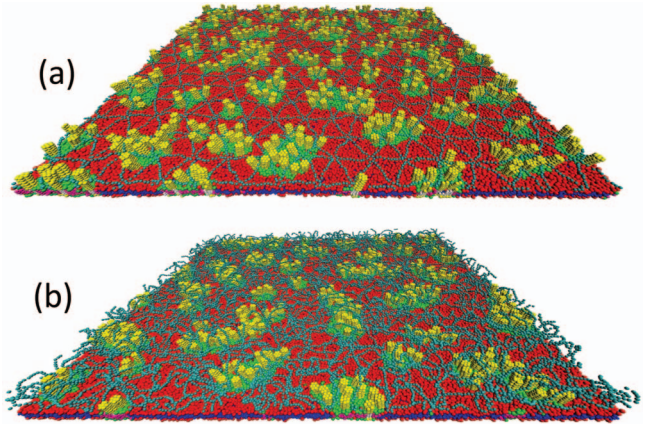

FIG. 8. Snapshot series for Set B systems containing 400 proteins at $20\,000\tau$. Panel (a) corresponds to the case of $\gamma_c = 1.06$ and (b) corresponds to $\gamma_c = 2.24$.

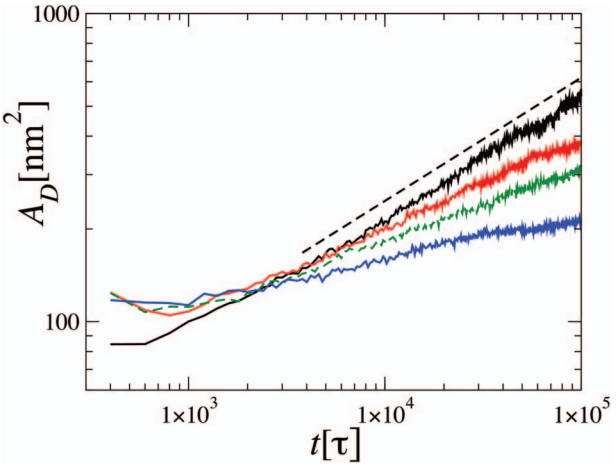

FIG. 9. Average domain area, A_D, *vs.* for Set B systems. Solid lines from top to bottom correspond to a pure binary bilayer (without proteins and cytoskeleton), $\gamma_c = 1.06$, $\gamma_c = 1.43$, $\gamma_c = 1.91$, and $\gamma_c = 2.24$, respectively. The slope of the dotted line is 0.4.

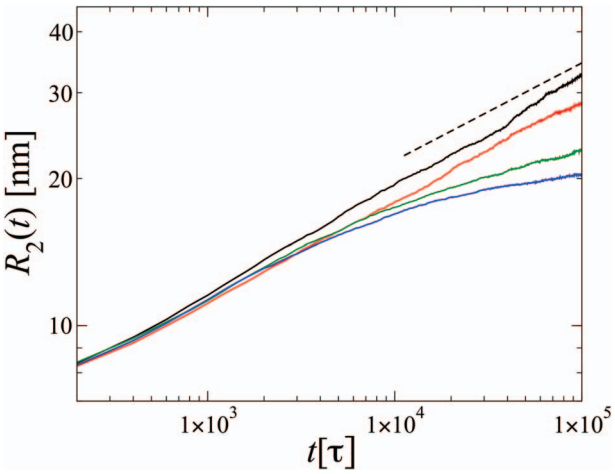

FIG. 10. Average domain size, R_2, *vs.* for Set C systems containing 400 proteins. Solid lines from top to bottom correspond to an average corral size $L_c \rightarrow \infty$ (no cytoskeleton), 41.80 nm, 20.90 nm, and 10.45 nm, respectively. The slope of the dotted line is 0.2.

are shown in Fig. 8 for the case of $N_p = 400$ with $\gamma_c = 1.06$ and 2.24. This figure shows that there are fewer domains in the case of a relaxed cytoskeleton than in the case of a tense cytoskeleton. In Fig. 9, the average domain area is shown vs. time for different values of the cytoskeleton proximity parameter for $N_p = 400$. This figure demonstrates that the growth of the average domain size is slowed down with increasing the cytoskeleton proximity parameter.

Our Set C simulations in which the number of proteins is $N_p = 400$, and the cytoskeleton proximity parameter is $\gamma_c = 1.06$, while the average corral size is varied show that the corral size also has a strong effect on the kinetics, as demonstrated by Fig. 10. In particular, we found that the domains growth rate is reduced with decreasing the average corral size. We note that even for the largest value of the corral size, $L_c = 41.80$ nm, the average domain size is expected to saturate at later times. However, the average domain size at saturation will be larger than the size of the simulation box, and cannot therefore be achieved with the current simulations.

IV. SUMMARY AND CONCLUSION

In this article, we presented results based on a computational study of the combined effects of transmembrane proteins and cytoskeleton on the dynamics of domain formation in multicomponent membranes. Specifically, we focused on lipid bilayers in the two-phase liquid-liquid coexistence containing transmembrane proteins with affinity to the minority lipid component. In this model, the proteins protrusion in the cytoplasmic side of the membrane makes them subject to steric hinderance by the cytoskeleton, with the degree of hindrance that depends on the cytoskeleton's proximity parameter, defined as the ratio between the arclength of the cytoskeleton strand between two anchors and the average end-to-end distance between two anchors. Our simulations are based on an implicit-solvent model with soft interactions that allows the lipids to self-assemble into bilayers, and with explicit proteins and cytoskeleton. The proteins in this model are mobile and the cytoskeleton is flexible. Our central result is that due to the favorable interaction between the proteins and one lipid phase and the steric hindering of the proteins by the cytoskeleton lead to microphase separation with an apparent domain size that decreases with increasing amount of proteins or corral size. We also found that the rate of domain growth is increased when the proximity parameter of the cytoskeleton is reduced. This is due to the fact that the protein diffusion is less hindered by the cytoskeleton when its proximity parameter is reduced, allowing for their escape, and therefore more coalescence of the protein-containing domains.

Our study is motivated by the fact that experimental evidence of hop diffusion of transmembrane proteins[60] and by the fact that transmembrane proteins are observed to cluster in regions enriched with cholesterol.[28] Our model is different from a previous phase field[34] and lattice models,[42–45] where the cytoskeleton's structure is time-independent, and in which the lipids directly interact with the cytoskeleton or with other lipids or proteins that are anchored to, and therefore immobilized by, the cytoskeleton. In these models, the observed microphase separation is due to the fact that the cytoskeleton effectively acts as a quenched disorder. As a result of this difference between our model and these models, the domains in our model are more compact, while the domains are interconnected in the previous models, faithfully conforming to the interconnected structure of the cytoskeleton. Most proteins in the plasma membrane are not anchored to the cytoskeleton, as demonstrated by their high diffusivity over short time and length scales. The confinement of most transmembrane proteins is the result of their hindered diffusion by the cytoskeleton rather than being rigidly attached to the cytoskeleton.

Our simulations were performed in the two phase region, while as demonstrated by Veatch *et al.*,[30] lipids in the plasma membrane might be close to the critical point. We plan to generalize our study to the critical region of the phase diagram, and detect how protein confinement and their affinity to liquid ordered regions affect the lateral lipid organization.

ACKNOWLEDGMENTS

We acknowledge the financial support from the National Science Foundation (Award Nos. DMR-0812470 and DMR-0755447) and the National Institute of General Medical Sciences of the National Institutes of Health (Award No. R15GM106326). The content is solely the responsibility of the authors and does not necessarily represent the official views of the National Institutes of Health.

[1] K. Simons and J. L. Sampaio, Cold Spring Harb. Perspect. Biol. **3**, a004697 (2011).
[2] K. Simons and G. Van Meer, Biochem. **27**, 6197–6202 (1988).
[3] L. J. Pike, J. Lipid Res. **47**, 1597–1598 (2006).
[4] K. Simons and E. Ikonen, Nature (London) **387**, 569–572 (1997).
[5] G. van Meer and H. Sprong, Curr. Opin. Cell Biol. **16**, 373–378 (2004).
[6] J. B. Helms and C. Zurzolo, Traffic **4**, 247–254 (2004).
[7] N. Chazal and D. Gerlier, Microbiol. Mol. Bio. Rev. **67**, 226–237 (2003).
[8] D. Raucher and M. P. Sheets, Biophys. J. **77**, 1992–2002 (1999).
[9] P. Sens and M. S. Turner, Phys. Rev. E **73**, 031918 (2006).
[10] L. A. Bagatolli and P. B. Sunil Kumar, Soft Matter **5**, 3234–3248 (2009).
[11] J. H. Ipsen, G. Kalström, O. G. Mouritsen, H. Wennerström, and M. J. Zuckermann, Biochim. Biophys. Acta **905**, 162–172 (1987).

[12]J. Silvius, D. del Giudice, and M. Lafleur, Biochem. **35**, 15198–15208 (1996).
[13]C. Dietrich, L. A. Bagatolli, Z. N. Volovyk, N. L. Thomson, M. Levi, K. Jacobson, and L. A. Gratton, Biophys. J. **80**, 1417–1428 (2001).
[14]S. L. Veatch and S. L. Keller, Phys. Rev. Lett. **89**, 268101 (2002).
[15]S. L. Veatch and S. L. Keller, Biophys. J. **85**, 3074–3083 (2003).
[16]T. Baumgart, S. T. Hess, and W. W. Webb, Nature (London) **425**, 821–824 (2003).
[17]S. L. Veatch and S. L. Keller, Phys. Rev. Lett. **94**, 148101 (2005).
[18]L. Li, X. Liang, M. Lin, and Y. Wang, J. Am. Chem. Soc. **127**, 17996–17997 (2005).
[19]M. Yanagisawa, M. Imai, T. Masui, S. Komura, and T. Ohta, Biophys. J. **92**, 115–125 (2007).
[20]A. R. Honerkamp-Smith, P. Cicuta, M. D. Collins, S. L. Veatch, M. den Nijs, M. Schick, and S. L. Keller, Biophys. J. **95**, 236–246 (2008).
[21]M. S. Bretscher, Nature New Biol. **236**, 11–12 (1972).
[22]G. van Meer and Q. Lisman, J. Biol. Chem. **277**, 25855–25858 (2002).
[23]J. Fan, M. Sammalkorpi, and M. Haataja, FEBS Lett. **584**, 1678–1684 (2010).
[24]J. Lin, A. Weiss, and T. S. Finco, J; Biol. Chem. **274**, 28861–28864 (1999).
[25]T. J. McIntosh, A. Vidal, and S. A. Simon, Biophys. J. **85**, 1656–1666 (2003).
[26]A. Kusumi, I. Koyama-Honda, and K. Suzuki, Traffic **5**, 213–230 (2004).
[27]S. J. Plowman, C. Muncke, R. G. Parton, and J. F. Kennedy, Proc. Natl. Acad. Sci. U.S.A. **102**, 15500–15505 (2005).
[28]B. F. Lillemeier, J. R. Pfeiffer, Z. Surviladze, B. S. Wilson, and M. M. Davis, Proc. Natl. Acad. Sci. U.S.A. **103**, 18992–18997 (2006).
[29]S. Mayor and M. Rao, Traffic **5**, 231–240 (2004).
[30]S. L. Veatch, P. Sengupta, A. Honerkamp-Smith, D. Holowka, B. Baird, and J. H. Freed, ACS Chem. Bio. **3**, 287–293 (2008).
[31]M. Laradji and P. B. Sunil Kumar, Phys. Rev. E **73**, 04901(R) (2006).
[32]S. Meinhardt, R. L. C. Vink, and F. Schmid, Proc. Natl. Acad. Sci. U.S.A. **110**, 4476–4481 (2013).
[33]L. Foret, Europhys. Lett. **71**, 508–514 (2005).
[34]J. Fan, M. Sammalkorpi, and M. Haataja, Phys. Rev. E **81**, 011908 (2010).
[35]K. Sornbundit, C. Modchang, W. Triampo, D. Triampo, and N. Nuttavut, Eur. Phys. J. Appl. Phys. **64**, 11101 (2013).
[36]R. Brewster and S. A. Safran, Biophys. J. **98**, L21–L23 (2010).
[37]C. Schroeder, H. Heider, E. Möncke-Buchner, and T.-I. Lin, Eur. Biophys. J. **34**, 52–66 (2005).
[38]J. S. Rossman, X. Jing, G. P. Leser, and R. A. Lamb, Cell **142**, 902–913 (2010).
[39]K. Weise, G. Triola, L. Brunsveld, H. Waldmann, and R. Winter, J. Am. Chem. Soc. **131**, 1557–1564 (2009).
[40]R. Brewster, P. P. Pincus, and S. A. Safran, Biophys. J. **97**, 1087–1094 (2009); **97**, 2115 (2009) (Erratum).
[41]K. Suzuki, K. Ritchie, E. Kajikawa, T. Fujiwara, and A. Kusumi, Biophys. J. **88**, 3659–3680 (2005).
[42]A. Yethiraj and J. C. Weisshaar, Biophys. J. **93**, 3113–3119 (2007).
[43]J. Gómez, F. Sagués, and R. Reigada, J. Chem. Phys. **132**, 135104 (2010).
[44]J. Ehrig, E. P. Petrov, and P. Schwille, Biophys. J. **100**, 80–89 (2011).
[45]B. B. Machta, S. Papanikolaou, J. P. Sethna, and S. L. Veatch, Biophys. J. **100**, 1668–1677 (2011).
[46]A. Honnigman, S. Sadeghi, J. Keller, S. W. Hell, C. Eggeling, and R. Vink, eLife **3**, e01671 (2014).
[47]N. Morone, T. Fujiwara, K. Murase, R. S. Kasai, J. Ike, S. Yuasa, J. Usukura, and A. Kusumi, J. Cell Biol. **174**, 851–862 (2006).
[48]J. D. Revalee, M. Laradji, and P. B. Sunil Kumar, J. Chem. Phys. **128**, 035102 (2008).
[49]E. J. Spangler, C. W. Harvey, J. D. Revalee, P. B. Sunil Kumar, and M. Laradji, Phys. Rev. E **84**, 051906 (2011).
[50]E. J. Spangler, P. B. Sunil Kumar, and M. Laradji, Soft Matter **8**, 10896 (2012).
[51]G. G. Putzel and M. Schick, Biophys. J. **95**, 4756–4762 (2008).
[52]R. S. Davis, M. M. Sperotto, P. B. Sunil Kumar, and M. Laradji, J. Phys. Chem. B **117**, 4072–4080 (2013).
[53]A. Khoshnood, H. Noguchi, and G. Gompper, J. Chem. Phys. **132**, 025101 (2010).
[54]M. Laradji and P. B. Sunil Kumar, Phys. Rev. Lett. **93**, 198105 (2004).
[55]M. Laradji and P. B. Sunil Kumar, J. Chem. Phys. **123**, 224902 (2005).
[56]S. Ramachandran, M. Laradji, and P. B. Sunil Kumar, J. Phys. Soc. Jpn. **78**, 041006 (2008).
[57]I. Pagonabarraga, M. H. J. Hagen, and D. Frenkel, Europhys. Lett. **42**, 377 (1998).
[58]K. Binder and D. Stauffer, Phys. Rev. Lett. **33**, 1006–1008 (1974).
[59]M. Laradji and M. J. A. Hore, J. Chem. Phys. **121**, 10641–10647 (2004).
[60]R. Simson, E. D. Sheets, and K. Jacobson, Biophys. J. **69**, 963–989 (1995).